Minimal Invasive Diagnostic Capabilities and Effectiveness of CFRP-Patches Repairs in Long-Term Operated Metals

Grzegorz Lesiuk [1,*] , **Bruno A. S. Pedrosa** [2] , **Anna Zięty** [1], **Wojciech Błażejewski** [1],
Jose A. F. O. Correia [3] , **Abilio M. P. De Jesus** [3] **and Cristiano Fragassa** [4]

[1] Department of Mechanics, Materials and Biomedical Engineering, Faculty of Mechanical Engineering, Wroclaw University of Science and Technology, Smoluchowskiego 25, PL-50-370 Wrocław, Poland; anna.ziety@pwr.edu.pl (A.Z.); wojciech.blazejewski@pwr.edu.pl (W.B.)

[2] ISISE, Departamento de Engenharia Civil, Universidade de Coimbra, Rua Luís Reis Santos, Pólo II, 3030-788 Coimbra, Portugal; bruno.pedrosa@uc.pt

[3] Faculty of Engineering, University of Porto, Rua Dr Roberto Frias, 4200-465 Porto, Portugal; jacorreia@inegi.up.pt (J.A.F.O.C.); ajesus@fe.up.pt (A.M.P.D.J.)

[4] Department of Industrial Engineering, University of Bologna, Viale Risorgimento 6, 40133 Bologna, Italy; cristiano.fragassa@unibo.it

* Correspondence: Grzegorz.Lesiuk@pwr.edu.pl; Tel.: +48-71-320-39-19

Abstract: The paper deals with the subject of diagnostics and the quick repairs of long-term operated metallic materials. Special attention was paid to historical materials, where the structure (e.g., puddle iron) is different from modern structural steels. In such materials, the processes of microstructural degradation occur as a result of several decades of exposure, which could overpass 100 years. In some cases, their intensity can be potentially catastrophic. For this reason, the search for minimally invasive diagnostic methods is ongoing. In this paper, corrosion and fracture toughness tests were conducted, and the results of these studies were presented for two material states: post-operated and normalized (as a state "restoring" virgin state). Moreover, through the use of modern numerical methods, composite crack-resistant patches have been designed to reduce the stress intensity factors under cyclic loads. As a result, fatigue lifetime was extended (propagation phase) by more than 300%.

1. Introduction

During the long-term operation of metallic materials and structures, the problem of their degradation becomes an issue, which could be serious when referring to bridge structures erected at the turn of the 19th to 20th centuries. This is the case of puddle iron, typically used in 19th-century metallic bridge structures, which is more susceptible to structural degradation processes than the old mild steel from the early 20th century. It is worth noting that in structural engineering at the beginning of the 20th century, both types of metallic materials were largely used. Nowadays, the maintenance and diagnostic of these old bridge structures, erected using puddle iron or old mild steel, is still a vital topic [1,2].

The puddle iron that was used as a constructional material is strongly influenced by local material flaws, which significantly limited the repairing techniques excluding (for instance) welding. Typically, the yield strength of puddle iron is about 250 ÷ 310 MPa, showing at a total elongation of

7 ÷ 25% [1–4]. Puddle iron has been characterized by variations in elongation, yield, and ultimate tensile strengths for the rolling direction as well as in the perpendicular direction. Therefore, puddle iron is often characterized by significant anisotropy of mechanical properties. In the rolling direction, they are significantly higher than in the direction perpendicular to it. This effect is a result of the former metallurgy process (puddling). However, it is more likely that this effect is strongly assisted by the degradation processes taking place in old steels [3–9] consisting, among others, of the decomposition of pearlite to ferrite and carbide, nitride, and carbide separations inside grains and at grain borders.

In order to illustrate the structure types and features indicating the degradation progress, all mentioned symptoms are documented in Figure 1, where the microstructures of steel from the Pomorski Środkowy and Północny Bridges located in Wrocław, Poland (Środkowy bridge erected in 1861–puddle iron, Północny bridge erected in 1930–mild steel) are shown. Figure 1a–d shows the typical microstructure of 19th-century puddle iron with numerous slags and nonmetallic inclusions (A) with brittle precipitations inside the ferrite grains (B) and a thick envelope of Fe_3C_{III} on the grain boundaries (C). The enlarged ferrite grains with degradation symptoms, brittle precipitations inside ferrite grains, are noticeable in Figure 1d. Due to the lack of a contemporary equivalent of the material from the 19th century, the normalization process is used as a heat treatment procedure simulating the original state of the material. However, if the degradation processes are very advanced, normalization does not remove all of the degradation products. This is a clear sign that the old material has been disposed of and this example is shown in Figure 1e.
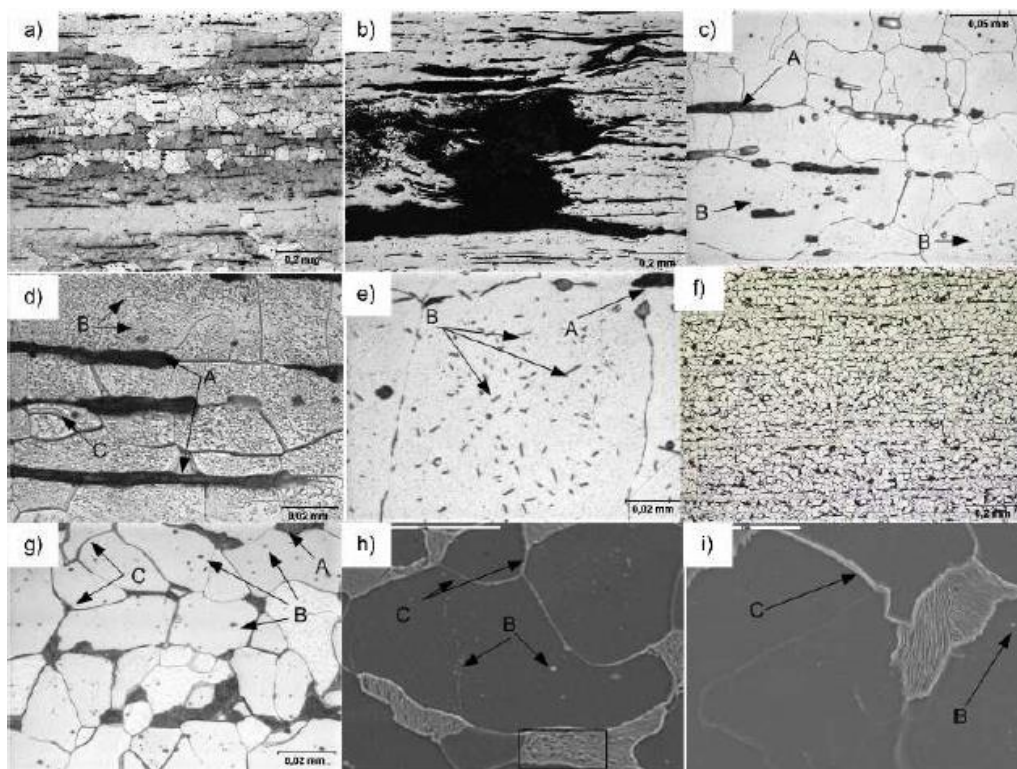

Figure 1. A typical microstructure of the long term-operated late 19th and early 20th century steels (described in the text). (**a**) typical microstructure of puddle iron, (**b**) enlarged non-metallic inclusion in puddle iron, (**c**) magnified microstructure of puddle iron, (**d**) magnified microstructure of puddle iron with microstructural degradation symptoms, (**e**) enlarged ferrite grain with degradation symptoms–puddle iron, (**f**) typical microstructure of early 20th century mild steel, (**g**) enlarged ferrite-pearlite microstructure of early 20th century mild steel, (**h**) SEM (Scanning Electron Microscope) image of early 20th century mild steel misstructure with small precipitations inside ferrite grains and degraded pearlites areas, (**i**) SEM (Scanning Electron Microscope) image of early 20th century mild steel misstructure without degradation symptoms.

The structural steels from the early 20th century (shown in Figure 1f–h) have a typical ferritic-pearlitic (A–pearlite areas) microstructure that is close to that of modern mild steels with small amounts of the degradation processes manifested in (B) brittle precipitations inside ferrite grains and degenerated pearlite areas (marked by frame). However, in the case of the presented early 20th-century mild steel, after normalization, the degradation symptoms disappeared (see Figure 1i). This type of structure leads to strain localization and makes the problem of fracture site prediction in the material more complex [6].

The presented microstructural features in old metallic materials also lead to significant changes in the fracture mechanisms visible in fractograms. Figure 2 illustrates the fracture surfaces of the specimens after Charpy testing for puddle iron and early 20th-century mild steel (the same materials as used for metallographic analysis from Figure 1).
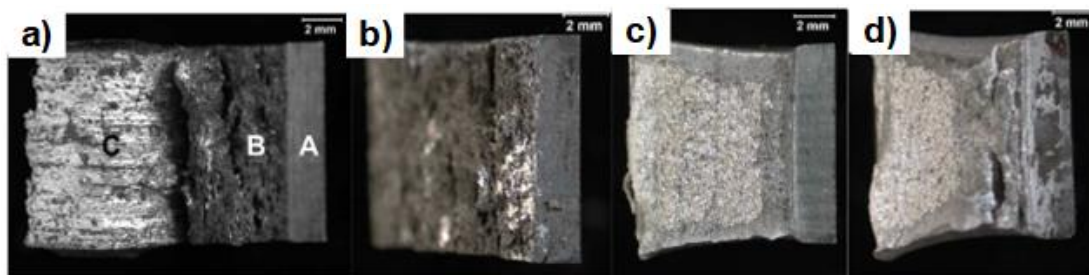

Figure 2. Fracture surfaces of the specimens after the Charpy impact test (+20 °C): (**a**) puddle iron in post-operated state (A–notch zone, B–crack propagation area, C–the plastic zone from the bottom part of the Charpy specimen), (**b**) puddle iron after heat treatment (normalized), (**c**) early 20th-century mild steel, post-operated state, (**d**) early 20th century mild steel, normalized state.

As shown in Figure 2, the differences in ductility were noticeable for both long-term operated materials. As reported in several papers devoted to the degradation of long-term operated materials, usually during maintenance service, two crucial issues have been raised [3–9]:

- How can we detect damage caused by material degradation using non-destructive or minimally invasive inspection at the operational level?
- How long can structures, mostly old steel structures, be operated under fatigue loads, and how can their service life be effectively extended temporarily until further repairs and renovations?

This article presents selected aspects of the strategy addressing the questions above in relation to historic long-term operated bridge steels.

2. Materials and Methods

Scientific investigations were conducted on 19th-century metallic materials extracted from the structural elements of a bridge built in the 19th-century in Bayonne, France (marked as "A" and subjected to fatigue crack growth tests. In 2013, it was demolished and replaced by a new bridge. The original one was mainly composed of puddle iron components through five spans (47 m + 3 × 60 m + 47 m) and a total length of 274 m. The main beams were formed with trusses in a Saint Andrew's cross shape that were 5.5 m high. After the disassembly of the bridge, several structural elements were preserved in order to perform scientific investigations. For corrosion and fracture toughness tests, we selected puddle iron (marked as "B") gained from the renovated 19th century Main Railway Station in Wrocław, Poland, as both materials had a similar chemical composition (reported in Table 1).

One group of materials was selected to test the degradation of the material and its potential impact on the susceptibility to brittle cracking. For this purpose, the crack resistance expressed as a critical integral *J* value was tested according to ASTM E1820 [10]. The main aim of the conducted works was to check if it would be possible to detect the material degradation phenomenon on the basis of corrosion tests

based on electrochemical parameters. In this group of samples, one part of the material was tested in the post-operative state and the other after heat treatment (normalization) to simulate the initial state. The relevance of such analysis has been widely confirmed by the authors' works concerning destructive mechanical tests [3–5,7,9], following the assumption of degradation theory [3,11,12]. For corrosion and fracture toughness tests, samples from the hall of the Wrocław Main Railway Station were used, resembling the materials published in the work (taken from other beams) [4].

Table 1. Chemical composition (% by weight) of the tested material compared with typical puddle irons and old mild steels.

Material	C	Mn	Si	P	S
puddle iron for fatigue crack growth rate (bridge from Bayonne, France) marked as "A"	<0.01	<0.02	0.28	0.41	0.054
Puddle iron from Main Railway Station (Wrocław, Poland) marked as "B"	0.02	0.03	0.13	0.29	0.048
typical values for puddle irons	<0.8	0.4	n/a	<0.6	<0.04
typical values for old mild steels	<0.15	0.2 ÷ 0.5	Variable	<0.06	<0.15

The second important contribution of this work was to develop a strategy for strengthening cyclically loaded structural members: crack repair with the use of composite materials. In this part of the study, the influence of the microstructural degradation phenomenon was not explicitly accounted. The problem of the degradation mechanism impact on fatigue lifetime reduction has been discussed in previous works by the authors [3–5]. However, it should be assumed that the reinforcement will work equally effectively in the post-operational state of the structure as well as after normalization, and the key elements of the research are the numerical analyses that allow for the correct design of the process to retard the development of fatigue-fracture by reducing the crack-like defect stress intensity factors (SIF). After the numerical part, fatigue crack growth laboratory tests were carried out on "hybrid" modified CT (Compact Tension)–metal–puddle iron (with comparable properties to the metal used in corrosion tests from the object tested in the work [13]) with adhesive and carbon fiber reinforced polymer (CFRP).

2.1. Corrosion Tests and Electrochemical Indicators of the Degradation Processes Activity

In order to perform corrosion tests, samples were carefully extracted using electro discharging machining (EDM) from parts of the steel structure. Special attention was paid to the extraction procedure in order not to lead to temperature changes. Before the main electrochemical measurement, each cylindrical sample (Figure 3) was degreased in acetone in an ultrasound bath for five minutes.
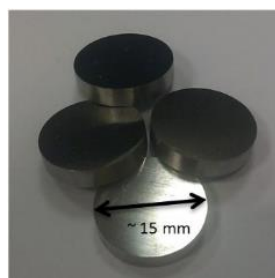

Figure 3. The geometry of the samples for the corrosion test.

Afterward, they were exposed for approximately 60 min in a corrosive medium of 3.5% NaCl solution. During this time, samples reached stability in the new environment. Samples prepared in this

way were tested in a three-electrode polarization measuring system. The fully automated test stand (Figure 4) consisted of a measuring vessel, the ATLAS 0531–Electrochemical UNIT & IMPEDANCE ANALYSER (ATLAS 0531 ELEKTROCHEMICAL UNIT & IMPEDANCE ANALYSER, Atlas-Sollich, Gdansk, Poland) potentiostat, and the computer drivers. The counter electrode was made of austenitic stainless steel, while the reference electrode was used as the electrode, a saturated Ag/AgCl. During the open circuit, potential measuring polarization curves were registered.
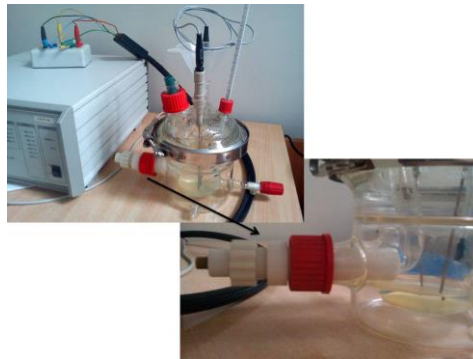

Figure 4. The electrochemical test stand used in the experimental campaign.

Moreover, the test was performed in the same polarity in the direction of the anode solution at a rate of $dE/dt = 1$ mV/s. The initial value of the potential was determined based on a stabilized value of the open circuit potential (E_0). All relevant parameters of corrosion current density (i_{corr}), corrosion potential (E_{corr}), Tafel coefficients ba and bc, and polarization resistance (R_p) were determined by the Stern method.

2.2. Fracture Toughness Tests

The tests were carried out using a MTS809 test machine, in accordance with ASTM E1820 [10], on the SEN (B) type three-point bend specimens with thickness $B = 10$ mm and width $W = 20$ mm. Mechanical notches were cut to a length of $a = 10.7$ mm using the EDM. Before the proper test, the fatigue pre-cracking procedure was involved according to ASTM E1820 [10]. For crack length calculation, an elastic-unloading compliance procedure was involved. Based on the registered signals of force, deflection, crack mouth opening displacement (CMOD), the J-R curves were evaluated, allowing the determination of the fracture toughness parameters expressed as critical values of the J integral.

2.3. Concept of the CFRP (Carbon Fiber Reinforced Polymer) Patches Strengthening and Numerical Analysis

The fatigue crack growth process is generally related to the severity of the stress distribution around the crack, which can be determined by the stress intensity factor. It is expected that using CFRP patches bonded to the material can contribute to decreasing the severity of the stresses around the crack tip, leading to an extension in fatigue life. Recent investigations have been performed in order to estimate the contribution of implementing the CFRP patch in CT specimens through numerical analysis. In recent considerations [14], different configurations of CFRP patches were studied (full-face and two strips) and numerical stress intensity factors were evaluated using X-FEM (eXtended Finite Element Method). However, in these studies, the adhesive was not modeled, and the interface between the CFRP and CT specimen was considered as perfectly tied, which means that there was no relative displacement in the interface. The crack in the CT specimens was imposed by node separation (X-FEM approach), and SIFs computed using the modified virtual crack closure technique (VCCT) for several imposed crack increments. In the present paper, numerical simulations were conducted to assess the values of the stress intensity factor for both strengthened and non-strengthened scenarios, as presented in Figure 5. The models were composed of a compact tension specimen with geometry

defined by W (width) equal to 50 mm and B (thickness) equal to 8.5 mm, a patch of CFRP, and an adhesive to establish the connection.
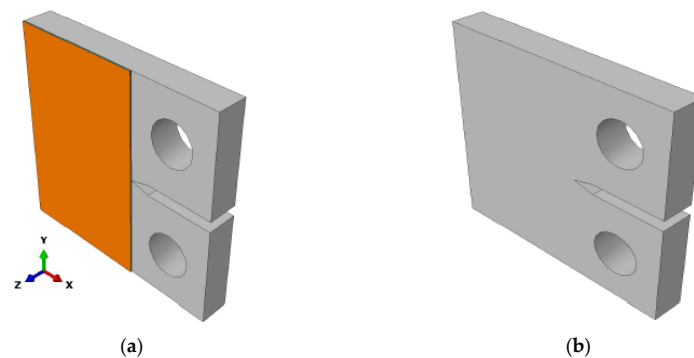

(a) (b)

Figure 5. Numerical models: (**a**) Strengthened compact tension (CT) specimen; (**b**) Plain steel CT specimen.

The metallic component was modeled with 3D finite elements with eight nodes, C3D8; the CFRP component was created using 3D shell elements with four nodes, S4; and the adhesive was modeled using 3D cohesive finite elements with eight nodes, COH3D8. Boundary conditions were set as pinned in the upper pin, $U_x = U_y = U_z = 0$, and as $U_x = U_z = 0$ for the lower pin. Loading was applied in the lower pin with a value equal to −7500 N in the y-direction. Boundary conditions and loads (Figure 6) were applied in reference nodes that are linked to the holes' surfaces by rigid links (kinematic coupling).
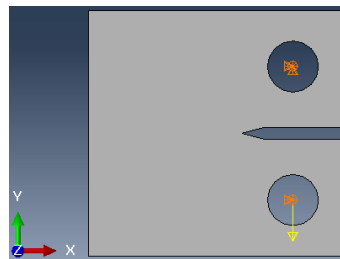

Figure 6. Boundary conditions and loads in the models.

Since the main objective of this study was to evaluate the stress intensity factor, an elastic fracture mechanics parameter and all the materials were set to linear elastic. In this sense, the metallic component was modeled with $E = 185$ GPa (typical average value within puddle iron [15]) and $v = 0.3$. The mechanical properties of the CFRP component were determined using the parameters for Sika® CarboDur® E-1014 (Sika Poland Sp. z o.o., Warszawa, Poland), as presented in Table 2. Direction 1 is the direction of the fibers and is aligned with direction y in Figures 5 and 6. The Young modulus in direction 2 (correlated with *x* in Figures 5 and 6) was considered as 10% of the main direction. The values of the shear moduli were defined using the data published by Naboulsi and Mall [16].

Table 2. Mechanical properties of CFRP (Carbon Fiber Reinforced Polymer) [17].

E_1 [GPa]	E_2 [GPa]	v_{12}	G_{12} [GPa]	G_{13} [GPa]	G_{23} [GPa]
170	17	0.17	7.24	7.24	4.94

For the adhesive component, the material law was defined with a cohesive mixed-mode damage model, as presented in Figure 7. It is characterized by a linear relation between stresses, *t*, and relative displacements, δ. The maximum value of stresses $t_{u,i}$ (*i* = I, II) defines the damage initiation and the

energy release rate, J_{ic}, is the parameter that gives the complete failure. In the case of mixed-mode behavior, damage initiation is based on the following quadratic stress criterion:

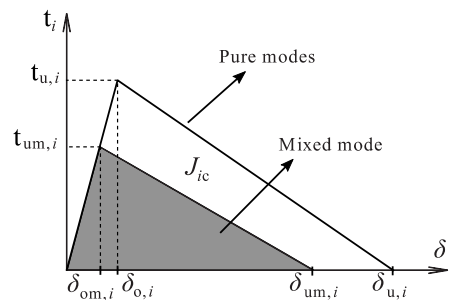$$\left(\frac{t_I}{t_{u,I}}\right)^2 + \left(\frac{t_{II}}{t_{u,II}}\right)^2 = 1 \tag{1}$$

Figure 7. Bilinear cohesive zone model for pure modes (I and II) and mixed-mode (I + II).

For the crack propagation, the following linear energetic criterion was used:

$$\frac{J_I}{J_{IC}} + \frac{J_{II}}{J_{IIC}} = 1 \tag{2}$$

The parameters of the model that was adopted in the analysis are described in Table 3.

Table 3. Mechanical properties of adhesive [18].

E [GPa]	ν [–]	$t_{u,I}$ [MPa]	$t_{u,II}$ [MPa]	J_{IC} [N/mm]	J_{IIC} [N/mm]
11.5	0.3	30	18	0.35	1.1

A total of four analyses were conducted in order to compute the stress intensity factor for different values of crack length: 15.5 mm, 18.5 mm, 21.5 mm, and 24.5 mm. The evaluation of this parameter was done using the modified virtual crack closure technique (VCCT) [19].

Recent studies have shown that as fatigue crack grows on a subtract, a debonded area is created between the subtract and reinforcement [20]. The definition of this region is presented in Figure 8. The parameter b is obtained by Equation (3), where a refers to the total crack length, a_0 is the distance between the loading axis and the CFRP patch (12.5 mm), and r_p is the plastic zone ahead of the crack tip, which can be calculated from Equation (4).

$$b = a - a_0 + r_p \tag{3}$$

$$r_p = \frac{1}{\pi}\left(\frac{K_{max}}{f_y}\right)^2 \tag{4}$$

The application of the modified VCCT allows for the computation of stress intensity factors in all points through-thickness of the crack tip. The validation of the method and the influence of the mesh were assessed by comparing the values of the stress intensity factors obtained for the non-strengthened model with the analytical solution presented in the ASTM E 647 standard for fatigue crack growth tests [21]:

$$\Delta K = \frac{\Delta P}{B\sqrt{W}}\frac{(2+\alpha)}{(1-\alpha)^{1.5}}\left[0.886 + 4.64\alpha - 13.32\alpha^2 + 14.72\alpha^3 - 5.6\alpha^4\right] \tag{5}$$

where α is the ratio a/W with a as the corresponding crack length measured during the test; ΔP is the applied force range; B is the thickness of the specimen; and W is the width.
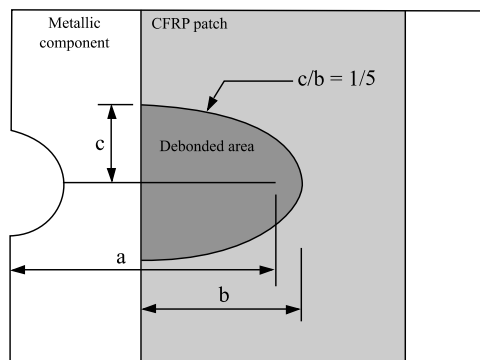

Figure 8. Definition of the debonded area.

The values of the stress intensity factor in the nodes through the thickness of the CT specimen (all points are shown in Figure 9) can be observed in Figure 10. In these graphics, node 1 is the node in the surface of the CT specimen, which is not reinforced with the CFRP patch, and node 29 is the opposite node situated in the face where the CFRP patch is bonded (see Figure 9). It is observed that the application of the CFRP patch produces a reduction on the stress intensity factor in all nodes of the crack tip.
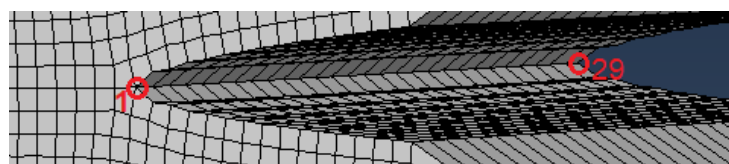

Figure 9. Mesh of the bare steel CT specimen: identification of node number through crack thickness.
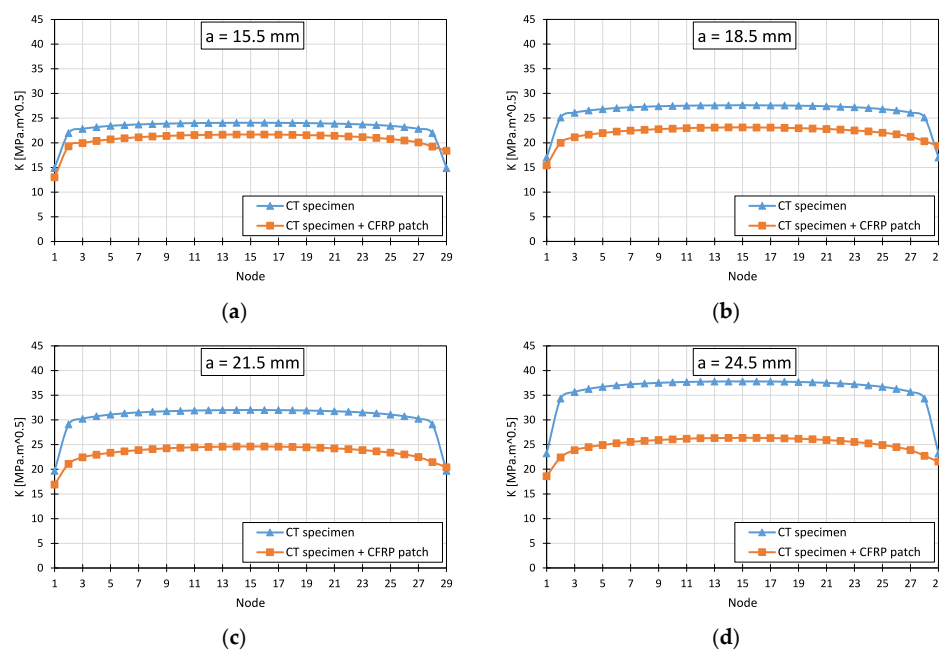

Figure 10. Numerical stress intensity factors for the strengthened and non-strengthened CT specimens, (**a**) variations of stress intensity factors (SIF) for crack length 15.5 mm, (**b**) variations of stress intensity factors (SIF) for crack length 18.5 mm, (**c**) variations of stress intensity factors (SIF) for crack length 21.5 mm, (**d**) variations of stress intensity factors (SIF) for crack length 24.5 mm.

Another important aspect that can be concluded from these graphics is that the difference between the stress intensity factors of strengthened and non-strengthened solutions increases for higher values of crack length. In fact, as presented in Table 4, the reduction on the stress intensity factor increased from 9% for a crack length equal to 15.5 mm to 32.3% for a crack length equal to 24.5 mm. In fact, the reduction of stress intensity factor is marginal for short cracks because the stiffness of the steel plate is much higher than that of the CFRP strips. However, the effectiveness of the patch reinforcement is maximized for long cracks because the patch covers a larger amount of the crack and its plastic zone. On average, the use of the CFRP patch led to a reduction in the stress intensity factor by 21%. Figure 11 and Table 4 present the evolution of the stress intensity factor with the crack length. It is shown that the numerical computation of stress intensity factors is in line with the analytical values and the difference varied between 0.9 and 2.7%.

Table 4. Comparison of final stress intensity factors.

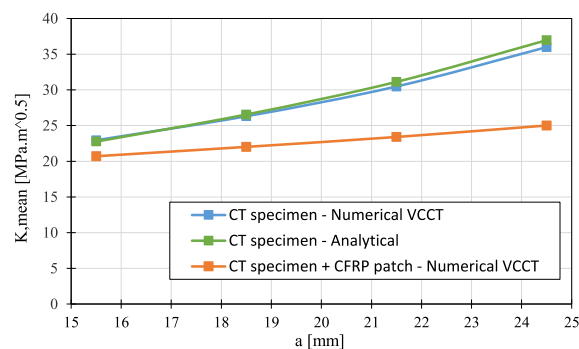| Crack Length	CT Specimen			CT Specimen + CFRP Patch	
	K [MPa*m$^{0.5}$]		Dif. (%)	K [MPa*m$^{0.5}$]	Dif. (%)
a [mm]	Analytical	Numerical VCCT		Numerical VCCT	
15.5	22.8	23.0	0.9%	20.7	9.0%
18.5	26.6	26.3	0.9%	22.0	17.1%
21.5	31.1	30.5	2.1%	23.4	24.8%
24.5	37.0	36.0	2.7%	25.0	32.3%

Figure 11. Comparison of final stress intensity factors.

3. Experimental Results and Discussion

3.1. Corrosion Resistance

Corrosion tests were performed for materials gained from the Main Railway Station (Wrocław, Poland, mechanical tests reported in [4]). Specimens marked as B1P mean that it is a material (puddle iron) from the Main Railway Station (Wrocław, Poland) in the post operated state, B1N are materials (puddle iron) from the Main Railway Station (Wrocław, Poland) after normalization. All electrochemical parameters for such material are shown in Figure 12. Analyzing the obtained values of E_0 and E_{corr} for the first group, their increase was observed. As presented in Figure 12, the parameters of samples after the normalizing process are increasing from about 10 mV for E_0 to almost 20 mV for values of E_{corr}. Moreover, *Rp* value also indicates a significant increase. According to the literature rule, when values of a potential and a resistant rise, the value of current should decrease.
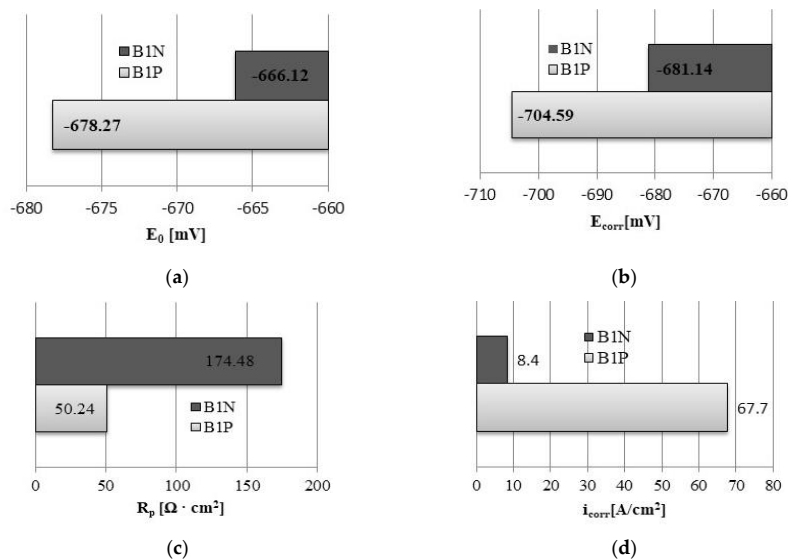
Figure 12. Results of the main parameters of electrochemical tests: (**a**) open circuit potential, (**b**) corrosion potential, (**c**) polarization resistance, (**d**) corrosion current density.

A higher corrosive resistance for samples with normalized conditions was also observed on the obtained polarization curves (Figure 13).
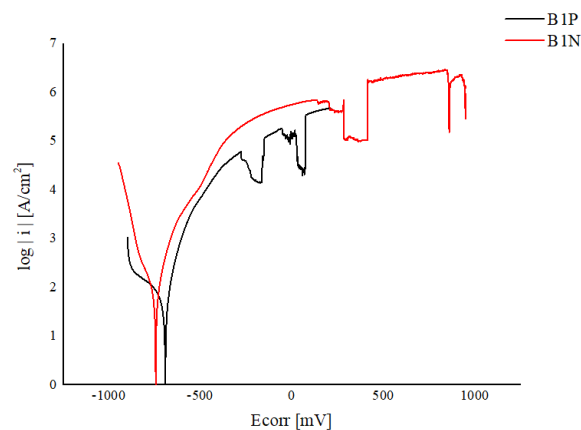

Figure 13. Polarization curves with the results of electrochemical tests for the B1P and B1N samples, where B1P is a post-operated state and B1N is a specimen after normalization.

3.2. Fracture Toughness Analysis: J Integral

According to the ASTM E1820 [10] recommendations, the J-R curves were drawn in Figure 14 for material in a post operated state and after heat treatment-normalization. The values of engineering J-integral $J_{0.2}$ were also determined. In Figure 14, there are marked horizontal lines corresponding with the J integral for the crack onset of 0.2 mm. However, because the thickness of 19th-century structural elements does not usually exceed 18 mm (in our case 10 mm), the plane strain condition cannot be achieved. In the presented results, the critical J_C values can be treated only (!) as a substitute (conditional) material resistant to cracking. The analysis of the experimental data showed that in the normalized state, the integral value of J_c was estimated on level $J_c = 104\,\text{N/mm}$, and in the post-operated state at $J_c = 87\,\text{N/mm}$. Comparing it with modern mild, low carbon steels, these values were far below the critical J integral, for example, S235/355 grade steel is $J_{IC} = 320\text{--}360\,\text{N/mm}$. By also analyzing the archival data [22–25] for a wide group of degraded materials (including pipeline steels), it is very likely that the applied corrosion testing method should find a non-invasive application in the detection of degradation damage. This shift in polarity curves and the change in the value of electrochemical

parameters of steel including 19th-century puddle iron could be a good indicator in the assessment of material exploitation level.
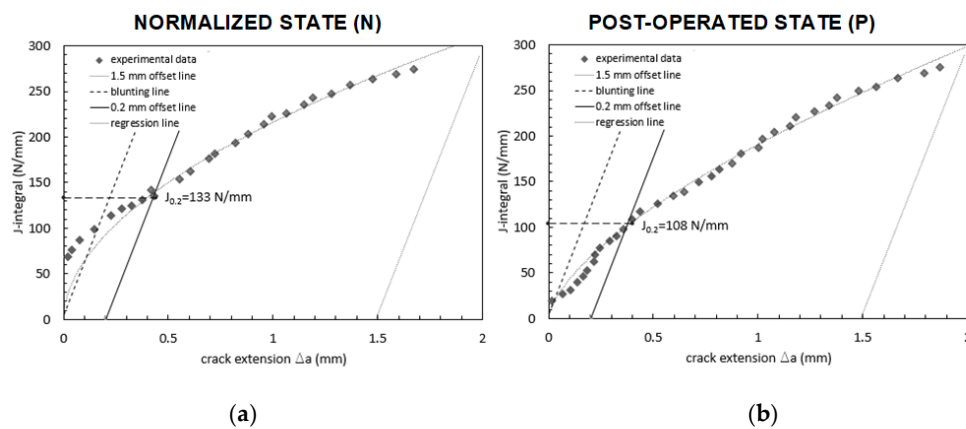

Figure 14. J-R curves for puddle iron after normalization heat treatment (**a**) and in the post-operated state (**b**).

Figure 14 clearly demonstrates the higher fracture resistance for the normalized state than for the post-operated state. After normalization, the critical J_c parameter increased by almost 20% and $J_{0.2}$ was −23% compared to the post-operated state.

3.3. Fatigue Crack Growth Test Results

The experimental campaign followed a numerical analysis of SIF and the influence of the CFRP patch on the SIF reduction. The geometry of CT specimens was defined as in the previous part, by W (width) = 50 mm and B (thickness) = 8.5 mm, as presented in Figure 15. The notch was created using electrical discharge machining. A preliminary FCG (Fatigue Crack Growth Rate) test produced the pre-crack under ΔK control with a maximum value of 15 MPa*m$^{0.5}$. To evaluate the influence of the mean stress effect, for non-strengthened specimens, different values of the stress ratio were used: 0.05, 0.1, and 0.7. During the tests of the fully metallic specimens, the crack length was monitored using the compliance method prescribed in the standard. The crack opening displacement and the applied force were also recorded in order to assess the effective stress intensity factor. Strengthened CT specimens were tested with the geometry and components described in Figure 15. The CFRP patch was glued in one face of the specimen with the fibers oriented perpendicular to the crack growth direction (parallel to the load application line). These tests were conducted under constant amplitude loading with a maximum value of 7500 N and a frequency of 10 Hz.
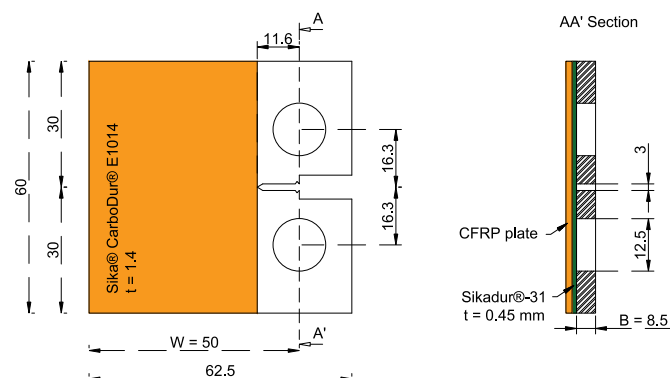

Figure 15. Geometry of CT specimens strengthened with the CFRP patch (all dimensions in mm).

The elaboration of FCG tests enabled us to compute the material parameters related to the crack growth resistance. In Figure 16, it is possible to observe the data obtained from FCG tests on non-strengthened specimens. It can be stated that the stress ratio influences the growth behavior since the data obtained for the stress ratio equal to 0.7 were significantly distinct from the data obtained for stress ratio equal to 0.05 and 0.1. While in the first case the constants C and m were 5.63×10^{-45} and 3.61, for the second case, the constants assumed the values 2.28×10^{-22} and 6.07. The following graphic represents the evolution of the crack growth curves using applied and effective stress intensity factors. It was observed that all the tests performed converged for one line when the effective stress intensity factors were used, computed using the compliance information.
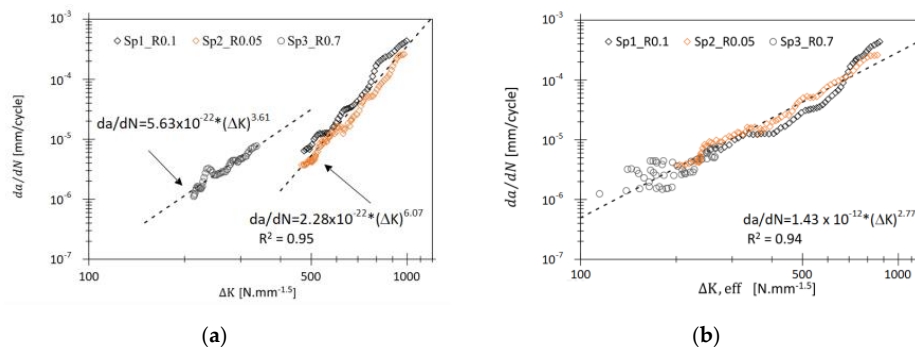

(a)   (b)

Figure 16. Fatigue crack growth data for the CT specimens: (**a**) use of applied stress intensity factors; (**b**) use of effective stress intensity factors.

In the case of the CT specimens strengthened with CFRP patches, the crack length was monitored using a microscope in the face with no patch. Figure 17 presents the evolution of the crack growth throughout the test performed under $R = 0.1$ and $F_{max} = 7500$ N. Comparing the data obtained from the FCG tests on strengthened specimens with the a-N curve defined by the material parameters determined with FCG tests on non-strengthened CT specimens, it is possible to state that the implementation of a CFRP patch led to a fatigue life extension of 318%.
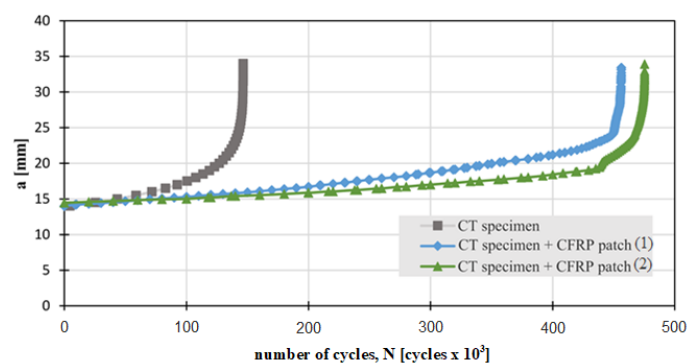

Figure 17. Crack growth evolution for strengthened and non-strengthened solutions ($R = 0.1$ and $F_{max} = 7500$ N).

4. Conclusions

The paper presents the diagnostic role of corrosion testing in the detection of degradation phenomena in the long-term operated metals. It also focuses on the capabilities of repairing metallic structures through the CFRP application. The following conclusions and observations can be made based on the performed investigations:

- shifting of polarization curves and change of electrochemical parameters are a good indicator to evaluate the operating condition of metals in the presented case puddle iron (19th century);

- in the case of puddle iron (and early mild steels), comparative analysis in the post-operated and normalized state—in the absence of material in the virgin state—is a reasonable solution to confirm the presence of microstructural degradation phenomena;
- application of modern adhesive solutions and CFRP patches allow effectively decelerating the development of fatigue cracking, which was confirmed numerically and experimentally. A prerequisite is to design the hybrid joint (metal + composite) correctly using numerical methods;
- further work will aim to establish the relationship between the fracture mechanism and diagnostic methods of structural elements subjected to multi-axial stress; and
- the future linking of changes in the electrochemical parameters of steel to the progress of degradation is also a further condition for the development of a diagnostic system for long term-operated materials, which requires even more experimental work. However, this study has shown the possible direction of further research.

Author Contributions: Conceptualization, G.L. and B.A.S.P.; Methodology, W.B. and J.A.F.O.C.; Validation, G.L. and C.F.; Formal analysis, A.M.P.D.J.; Investigation, G.L. and A.Z.; Resources, C.F.; Data curation, G.L. and A.Z.; Writing—original draft preparation, G.L. and B.P.; Writing—review and editing, G.L., J.A.F.O.C., and C.F.; Visualization, A.Z. and B.P.; Supervision, G.L. and C.F.; Project administration, G.L.; Funding acquisition, G.L. All authors have read and agreed to the published version of the manuscript.

Conflicts of Interest: The authors declare no conflict of interest.

References

1. Hołowaty, J. Toughness tests on steels from old railway bridges. *Procedia Struct. Integr.* **2017**, *5*, 1043–1050. [CrossRef]
2. Sieber, L.; Stroetmann, R. The brittle fracture behaviour of old mild steels. *Procedia Struct. Integr.* **2017**, *5*, 1019–1026. [CrossRef]
3. Lesiuk, G.; Correia, J.A.F.O.; Krechkovska, H.V.; Pekalski, G.; Jesus, A.M.P.; de Student, O. Degradation Theory of Long Term Operated Materials. In *Structural Integrity Series*; Springer Nature: Heidelberg, Germany, 2021; Volume 15, in press.
4. Lesiuk, G.; Szata, M.; Bocian, M. The mechanical properties and the microstructural degradation effect in an old low carbon steels after 100-years operating time. *Arch. Civ. Mech. Eng.* **2015**, *15*, 786–797. [CrossRef]
5. Lesiuk, G.; Szata, M. Aspects of structural degradation in steels of old bridges by means of fatigue crack propagation. *Mater. Sci.* **2011**, *47*, 82. [CrossRef]
6. Balokhonov, R.; Romanova, V. On the problem of strain localisation and fracture site prediction in materials with irregular geometry of interfaces. *Facta Univ. Ser. Mech. Eng.* **2019**, *17*, 169–180.
7. Krechkovska, H.; Student, O.; Lesiuk, G.; Correia, J. Features of the microstructural and mechanical degradation of long term operated mild steel. *Int. J. Struct. Integr.* **2018**, *9*, 296–306. [CrossRef]
8. Zvirko, O.I.; Mytsyk, A.B.; Tsyrulnyk, O.T.; Gabetta, G.; Nykyforchyn, H.M. Corrosion degradation of steel of long-Term operated gas pipeline elbow with large-scale delamination. *Mater. Sci.* **2017**, *52*, 861–865. [CrossRef]
9. Szata, M.; Lesiuk, G.; Pękalski, G. Assessment of degrading processes progress in the old brigde steel in terms of fracture mechanics-Part one-The investigation of possibilities. *Logistyka* **2009**. bwmeta1.element.baztech-article-BUS6-0035-0025. Available online: http://yadda.icm.edu.pl/yadda/element/bwmeta1.element.baztech-article-BUS6-0035-0025 (accessed on 12 May 2020).
10. ASTM E1820; *Standard Test Method for Measurement of Fracture Toughness*; American Society for Testing and Materials: West Conshohocken, PA, USA.
11. Dudziński, W.; Konat, Ł.; Pękalski, G. Modern constructional steels. In *Maintenance Strategy of Surface Mining Machines and Facilities with High Technical Degradation Levels*; Wrocław, D.D., Ed.; Publishing House of Wrocław University of Technology: Wrocław, Poland, 2013; pp. 346–366.
12. Konat, Ł.; Pękalski, G. Overview of Materials Testing of Brown-Coal Mining Machines (Years 1985–2017). In *Mining Machines and Earth-Moving Equipment*; Springer: Heidelberg, Germany, 2020; pp. 21–58.

13. Lesiuk, G.; Sire, S.; Ragueneau, M.; Correia, J.A.F.O.; Pedrosa, B.A.S.; Jesus, A.M.P. Mean Stress Effect and Fatigue Crack Closure in Material from Old Bridge Erected in the Late 19th Century. *Procedia Struct. Integr.* **2019**, *17*, 198–205. [CrossRef]

14. Lesiuk, G.; Katkowski, M.; Correia, J.; De Jesus, A.; Blazejewski, W. Fatigue Crack Growth Rate in CFRP Reinforced Constructional Old Steel. *Int. J. Struct. Integr.* **2018**, *9*, 381–395. [CrossRef]

15. Lesiuk, G.; Kucharski, P.; Correia, J.; De Jesus, A.; Rebelo, C.; Simões da Silva, L. Mixed Mode (I+II) Fatigue Crack Growth in Puddle Iron. *Eng. Fract. Mech.* **2017**, *185*, 175–192. [CrossRef]

16. Naboulsi, S.; Mall, S. Modelling of a Cracked Metallic Structure with Bonded Composite Patch Using the Three Layer Technique. *Compos. Struct.* **1996**, *35*, 295–308. [CrossRef]

17. *Sika Product Data Sheet: Sika® CarboDur® E-1014*; Sika Sp. z. o.o.: Warsaw, Poland, 2019.

18. Dourado, N.; Pereira, F.A.M.; de Moura, M.F.S.F.; Morais, J.J.L. Repairing Wood Beams under Bending Using Carbon-Epoxy Composites. *Eng. Struct.* **2012**, *34*, 342–350. [CrossRef]

19. Krueger, R. Virtual Crack Closure Technique: History, Approach, and Applications. *Appl. Mech. Rev.* **2004**, 109–143. [CrossRef]

20. Karbhari, V. *Rehabilitation of Metallic Civil Infrastructure Using Fiber-Reinforced Polymer (FRP) Composites*; Woodhead, P., Ed.; Elsevier: Cambridge, UK, 2014.

21. ASTM E 647; *Standard Test Method for Measurement of Fatigue Crack Growth Rates*; American Society for Testing and Materials: West Conshohocken, PA, USA, 2015.

22. Gallegos Mayorga, L.; Sire, S.; Ragueneau, M.; Plu, B. Understanding the Behaviour of Wrought-Iron Riveted Assemblies: Manufacture and Testing in France. In *Proceedings of the Institution of Civil Engineers-Engineering History and Heritage*; ICE Publishing: London, UK, 2017; Volume 170, pp. 67–79.

23. Zvirko, O.; Nykyforchyn, H.; Szata, M.; Kutnyi, A.; Lesiuk, G. Corrosion degradation of old structures steels. In *XII International Conference "Problems of Corrosion and Corrosion Protection of Structural Materials"*; Corrosion: Lviv, Ukraine, 2014.

24. Tsyrul'nyk, O.T.; Kret, N.V.; Voloshyn, V.A.; Zvirko, O.I. A procedure of laboratory degradation of structural steels. *Mater. Sci.* **2018**, *53*, 674–683. [CrossRef]

25. Zvirko, O.; Zagórski, A. Corrosion and electrochemical properties of the steel of exploited oil tanks in bottom water. *Mater. Sci.* **2008**, *44*, 126–132. [CrossRef]